# Physics of the off-Diagonal Momentum Flux

P.H. Diamond, UCSD and NFRI, G. Dif-Pradalier, and the Theory-Computation Joule Milestone Team*

**Abstract**

The task of this quarter was to elucidate the physics and advance predictive understanding of the off-diagonal contributions to the flux of toroidal momentum.

## I. Introduction and Summary of Issues

The aim of this portion of the Milestone activity was to elucidate the physics and advance the predictive understanding of the non-diffusive, off-diagonal contributions to the flux of toroidal momentum –including both pinch and residual stress pieces– and to address the relation between momentum and density pinches. Recall that the total flux of toroidal momentum driven by electrostatic turbulence has the form (c.f. Diamond et al, 2009[1]).

$$\Pi_{r,\phi} = \langle n \rangle \left( -\chi_\phi \frac{\partial}{\partial r} \langle v_\phi \rangle + V \langle v_\phi \rangle + \Pi_{r,\phi}\big|_{resid.} \right) + \langle v_\phi \rangle \Gamma_n \qquad \textbf{(1)}$$

Here $\chi_\phi$ is the turbulence momentum diffusivity induced by $\tilde{E} \times \tilde{B}$ scattering, $V$ is the convective flux or "pinch", and $\Pi_{r,\phi}\big|_{resid.}$ is the residual stress. Note that:

1.) the pinch, which is strongly suggested by several experiments (c.f. Yoshida et al, 2006 [2]; Tala et al, 2008[3]) reflects a $\nabla T_i$ , $\nabla n$ , or $\nabla T_e$ driven flux of momentum, in proportion to the existing mean flow. The pinch can be either turbulence equipartition (i.e. a consequence of $\nabla \cdot \left( \tilde{v}_{E \times B} \right) \neq 0$ in toroidal geometry) or thermoelectric. Examples

---

**C. McDevitt, C.J. Lee, UCSD; W. Wang, T.S. Hahm, E.S. Yoon, PPPL; S. Ku, C.S. Chang, CIMS-NYU; J.M Kwon, S. Yi, NFRI-ROK.

include work by Peeters et al. 2007[4]; Hahm et al. 2007, 2008[5]; Gurcan et al. 2008[6]; Yoon and Hahm, 2010[7].

2) the residual stress, which is required to address the phenomenon of intrinsic rotation, is a consequence of $\nabla P$, $\nabla T$ and $\nabla n$ driven Reynolds stress which acts without a pre-existing flow. The residual stress, which is conceptually different from a "pinch", is a consequence of wave-mean flow momentum exchange. The residual stress requires some form of symmetry breaking, due to mean and zonal $E \times B$ shear (Gurcan, Diamond et al, 2007[8]; also several groups made relevant suggestions in early 90's[9]), fluctuation intensity gradients (Gurcan et al., 2010[10]), plasma current (C. Lee et al., 2009[11]), plasma current poloidal asymmetry (Camenen et al., 2009[12]), etc. Note that some residual stress is required to explain intrinsic rotation experiments such as those of Solomon 2007, 2009[13] -i.e. to explain why one net counter-direction beam holds the plasma stationary with no net $\langle v_\phi \rangle$ or $\nabla \langle v_\phi \rangle$, to within the accuracy of measurements.

To address the focus of this quarter, namely a detailed elucidation of the physics of the off-diagonal components of the momentum flux, i.e. the residual stress $\Pi_{r,\phi}|_{resid.}$ and the pinch $V$, we note that the key issues are:

a) what is the basic physics of the residual stress, which is essential to the important phenomenon of intrinsic rotation? In particular, what are the relevant mechanisms of symmetry breaking and which are dominant under what circumstances?

b) what is the basic physics of the momentum pinch? In particular, how do TEP (Turbulent Equi-Partition, which will be explained further on the page 11), $\nabla T$

and $\nabla n$ effects compete to form $V$? How are $V_{\text{momentum}}$ and $V_{\text{density}}$ related?

This report addresses these issues by a discussion of relevant theory and simulation studies. The latter aim to probe and test the predictions made by the former, thus advancing the status of *predictive understanding*. The report is organized as follows:

- section II discusses the theory of the residual stress $\Pi_{r,\phi}\big|_{resid.}$ and the pinch $V$.

  Several new, previously unpublished results and ideas are presented.

- section III presents the computational results. They are organized as:

  i. basic issues and approaches

  ii. gKPSP studies [14]

  iii.GTS studies [15]

  iv.XGC studies [16]

  v. discussion of results.

  Several unpublished computational results are presented and discussed.

- section IV presents the conclusions. Areas where further research is needed are identified.

## II. Theory Summary

This section summarizes recent advances in the theory of the residual stress $\Pi_{r,\phi}\big|_{resid.}$ and of the pinch $V$. These are presented in Sections (II.A) and (II.B) respectively.

### 1. Theory of the Residual Stress

Intrinsic rotation is thought to be generated by $\nabla P$, $\nabla T$ or $\nabla n$-driven non-diffusive

wave stresses ('residual stress') which work against turbulent viscosity to drive mean flows. Some form of symmetry breaking is required to set the sense of the residual stress. Here, we summarize a comprehensive study of residual stress physics, which indicates that non-diffusive $\nabla P$ -driven wave stresses with broken symmetry are generic to, and ubiquitous in, heat flux driven, turbulent toroidal plasmas. Thus, it should not be surprising that intrinsic rotation is also ubiquitous. Wave turbulence can drive flows via:

i.) residual parallel Reynolds stress $\left\langle \tilde{V}_{rE}\tilde{V}_{\|} \right\rangle$ , which requires $k_{\|}$ symmetry breaking to un-balance toroidally counter-propagating acoustic wave populations. Broken symmetry $k_{\|}$ can be produced by a spectral shift, as for the oft-quoted case of $E \times B$ shear, or, by a spectral envelope intensity gradient, or by toroidal current. Note that recent simulation results, discussed in section III, suggest that $k_{\|}$ symmetry breaking is not exclusively correlated with mean $E \times B$ shear. Also, intensity profile gradients are ubiquitous, since fluctuation levels are usually observed to increase with radius. Intensity profiles are intrinsic to confinement, since at constant heat flux, negative temperature profile curvature (i.e. as for a pedestal) requires a decreasing intensity profile, while positive profile curvature (i.e. as for an L-mode edge) implies a rising intensity profile.

Proceeding in more detail, $k_{\|}$ symmetry breaking and residual stress can result from: a) electric field shear, b) current or c) intensity gradients.

**Regarding a)**, the essential physics is that $\langle V_E \rangle'$ converts poloidal flow shear to toroidal flow shear via asymmetry in wave-particle momentum deposition. The latter

results from the tendency of finite $\langle V_E \rangle'$ –working together with generic drift-acoustic coupling– to produce a shifted spectral envelope, so $\langle k_\parallel \rangle \neq 0$. Here $\langle k_\parallel \rangle = k_\theta \, \delta x / L_s$, where the spectral shift $\delta x \sim \langle V_E \rangle'$. The broken symmetry and $\langle k_\parallel \rangle \neq 0$ result in a directional imbalance of acoustic wave population and thus in the profile of momentum dissipation by ion Landau damping. The electric field shear symmetry breaking scenario is depicted in Fig.1.

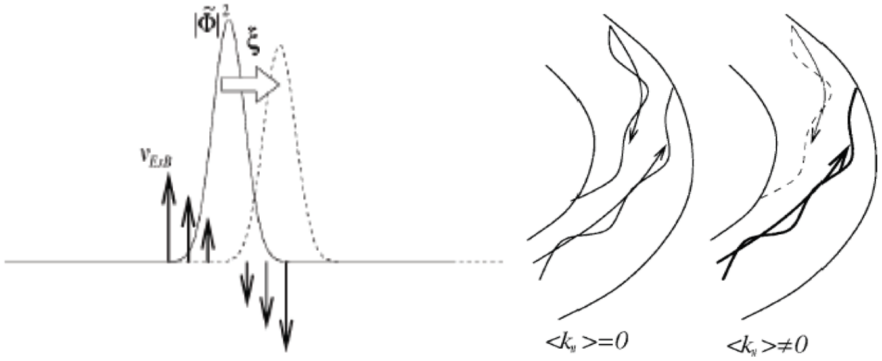


**Figure 1. The electric field shear symmetry breaking scenario [17]**

This process is a special case of the more general phenomenon of winding asymmetry-induced stress, which corresponds to the second term in the equation below, i.e.:

$$\Pi_{r,\parallel}^{wave} = \int d\mathrm{k}\; k_\parallel \left\{ -\tau_{c,\mathrm{k}} v_{gr}^2 \frac{\partial \langle N_\mathrm{k} \rangle}{\partial \mathrm{r}} + \tau_{c,\mathrm{k}} v_{gr} k_\theta \langle V_E \rangle' \frac{\partial \langle N_\mathrm{k} \rangle}{\partial \mathrm{k_r}} \right\} \qquad \textbf{(2a)}$$

The effective $\langle k_\parallel \rangle$ is in turn given by:

$$\frac{\partial}{\partial t}\langle k_\parallel \rangle = -\frac{1}{r}\frac{\partial}{\partial r}\left[ r \Pi_{r,\parallel}^{wave} \right] - \int d\mathrm{k}\; \frac{\partial k_\parallel}{\partial k_r} k_\theta \langle v_E \rangle' \langle N \rangle - \int \mathrm{kb} \cdot \vec{\mathrm{D}}_\mathrm{k} \cdot \nabla_\mathrm{k} \langle N \rangle + 2 \int d\mathrm{k}\; k_\parallel \gamma_k \langle N \rangle - \gamma_{NL} \langle k_\parallel \rangle \qquad \textbf{(2b)}$$

Note that the second term on the RHS accounts for symmetry breaking by shear-induced winding. This relationship is discussed further in Diamond et al., 2008[18]. Eq.(2a) gives

the flux of parallel wave momentum in the short mean free path limit. Term (1) on the RHS corresponds to intensity gradient driven radiative spatial diffusion of wave momentum. Term (2) on the RHS describes refraction induced wave quanta population imbalance. This effect is especially important in regimes of strong shearing, such as ETBs and ITBs. Note that Eq.(2a) may be re-written as:

$$\Pi_{r,\parallel}^{wave} = -D_w \frac{\partial \langle P_\parallel^w \rangle}{\partial \mathrm{r}} + V_w \langle P_\parallel^w \rangle \qquad \textbf{(2c)}$$

Here, $\langle P_\parallel^w \rangle = \int d\mathrm{k}\, k_\parallel \langle N \rangle$ is the parallel wave momentum;

$$D_w = \int d\mathrm{k}\, \mathrm{v}_\mathrm{g}^2 \tau_{c,\parallel} \langle N \rangle \Big/ \int d\mathrm{k}\, \langle N \rangle \qquad \textbf{(2d)}$$

is the wave radiative diffusivity and

$$V_w = \int d\mathrm{k}\, \frac{\partial}{\partial \mathrm{k}_\mathrm{r}} \left( v_{gr} \tau_{c,\parallel} \right) \mathrm{k}_\theta \langle \mathrm{v}_E \rangle' \langle N \rangle \Big/ \int d\mathrm{k}\, \langle N \rangle \qquad \textbf{(2e)}$$

is the convection velocity of parallel wave momentum. Observe that Eq.(2b) gives an illuminating expression for the non-resonant piece of the residual stress. The resonant particle residual stress is discussed in Diamond et al., 2008[18]. In general, the non-resonant residual stress will be stronger.

**Regarding b)** asymmetric spectral shifts may be produced by current, as for the well-known case of resistivity gradient driven turbulence or rippling models. These models, and others like them, are intrinsically asymmetric about resonant surfaces. For current driven drift waves, $\langle k_\parallel \rangle \sim v_d / c_s$ where $v_d$ is the mean electron drift velocity.

**Regarding c)** it is not difficult to see that *any* intensity gradient results in effective $k_\parallel$ symmetry breaking. This follows from the fact that, schematically (here $\mathrm{r}_0$ is the resonant surface radius):

$$\Pi_{r,\phi}^{resid} \cong \left\langle k_\theta k_\parallel \left|\Phi_k\right|^2 \right\rangle$$
$$\cong \left\langle k_\theta^2 \frac{(r-r_0)}{L_s} \left\{ \left|\Phi_k(r_0)\right|^2 + (r-r_0)\frac{\partial}{\partial r}\left|\Phi_k(r_0)\right|^2 + ... \right\} \right\rangle \qquad \textbf{(3)}$$
$$\cong \left\langle k_\theta^2 \frac{(r-r_0)^2}{L_s} \frac{\partial}{\partial r}\left|\Phi_k(r_0)\right|^2 \right\rangle$$

Here, $\left\langle (r-r_0)^2 \right\rangle \to \left\langle \Delta^2 \right\rangle$, where $\Delta$ is the spectral width. Note that an intensity gradient is a very general phenomenon, which will occur whenever the temperature gradient has finite curvature, for constant heat flux. This follows from $Q = -\chi_i \partial \langle T_i \rangle / \partial r$ , where $\chi_i = \chi_{i,turb} + \chi_{i,NC}$, so fixed heat flux gives $\partial Q / \partial r = 0$ and

$$\frac{\partial \chi_{i,turb}/\partial r}{\chi_i} = -\frac{\partial^2 \langle T \rangle / \partial r^2}{\partial \langle T \rangle / \partial r} - \frac{\partial \chi_{i,NC}/\partial r}{\chi_i} \qquad \textbf{(4)}$$

Since $\chi_{i,turb} \sim \left|\Phi_k\right|^2$ , the connection between intensity gradients and profile curvature follows. Intensity gradients are especially likely to occur near transport barriers, where electric field shear can be strong as well. Thus, there will likely be strong overlap and mutual reinforcement between these two effects. In particular, since the electric field shearing rate: $\langle v_E \rangle' = \frac{P_i''}{nq} - \frac{P_i' n'}{n^2 q} + v_\phi' B_\theta - v_\theta' B_\phi$ , we see that *both* $\langle v_E \rangle'$ and intensity gradient $I'$ are ultimately related to the temperature profile curvature.

ii.) mean radial current $\left(\langle J_r \rangle\right)$ driven toroidal torques $\left(\sim \langle J_r \rangle B_\theta / c\right)$, induced by the radial

flux of polarization charge [19]. Ultimately, this process drives a net effective stress $\left\langle \tilde{V}_{rE}\tilde{V}_{\theta}\right\rangle B_{\theta}/B_{T}$ . Hereafter, we consider only **ExB** flows for simplicity. Diamagnetic corrections will be discussed in Quarter 4. **A** finite Reynolds stress $\left\langle \tilde{V}_{rE}\tilde{V}_{\theta}\right\rangle$ requires either a diffusive flux of poloidal wave momentum or modulational instability feedback amplifier based on $E\times B$ shear-induced wave refraction, as is the case for zonal flow growth. These mechanisms work via spectral symmetry breaking in either $r$ ($\partial\langle N\rangle/\partial r\neq 0$) or $k_r$ ($\partial\langle N\rangle/\partial k_r\neq 0$). Here $N$ refers to the wave action density. Due to the fragility of the $k_{\|}$ symmetry breaking mechanisms, the $\langle J_r\rangle$-driven residual stress is, in general, stronger than the $\left\langle \widetilde{V}_{rE}\widetilde{V}_{\|}\right\rangle$ driven residual.

Regarding radial current, detailed analysis gives the net toroidal force as:

$$\langle J_r\rangle\frac{B_{\theta}}{c}=\frac{B_{\theta}}{B_0}\frac{\partial}{\partial r}\Pi_{r,\perp}^{wave} \qquad \textbf{(5)}$$

where $\Pi_{r,\perp}^{wave}$ is the radial-perpendicular (binormal) stress induced by waves. Note that Eq. (5) effectively states that radial current-induced force is equivalent to a toroidal projection of the perpendicular stress. Now, since the latter is a wave stress:

$$\frac{B_{\theta}}{B_T}\frac{\partial}{\partial r}\Pi_{r,\perp}^{wave}=\frac{B_{\theta}}{B_0}\frac{\partial}{\partial r}\sum_{\|}v_{gr}k_{\theta}N_{\|} \qquad \textbf{(6)}$$

so, standard wavekinetic analysis then yields:

$$\Pi_{r,\perp}^{wave}=-D_w\frac{\partial\langle P_{\theta}\rangle}{\partial \mathrm{r}}+\alpha\langle v_E\rangle' \qquad \textbf{(7a)}$$

where:

$$D_w = \sum_{\|} v_{gr,\mathrm{k}}^2 \tau_{c,\mathrm{k}} \qquad \textbf{(7b)}$$

is the wave packet radiative diffusivity and $\langle P_\theta \rangle$ is the wave poloidal momentum (i.e. pseudomomentum). Similarly, $\alpha \langle v_E \rangle'$, where

$$\alpha = -\sum_{\|} \frac{2k_\theta^2 \rho_s^2 \tau_{c,\mathrm{k}}}{\left(1 + k_\perp^2 \rho^2\right)^2} k_r \frac{\partial}{\partial k_r} \langle \Omega \rangle, \quad \textbf{(7c)}$$

is the electric field shear driven wave momentum flux. Here $\langle \Omega \rangle$ is the wave enstrophy density. Note that the term $\alpha \langle v_E \rangle'$ is effectively identical to that which produces zonal flow growth (i.e. modulational instability). Observe that the upshot of this analysis is that the radial transport of toroidal momentum can occur both via:

a. radial transport of parallel momentum

b.the toroidal projection of the radial flux of *perpendicular* momentum

In general, the comparison of these two can be reduced to a comparison of $\langle k_\| \rangle$ and $\overline{k_\theta} B_\theta / B_T$, where $\overline{k_\theta} = k_{\theta,RMS}$. Since it is virtually always the case that $r > \hat{s}\, \delta x$ (i.e. $\delta x$ is the $\langle v_E \rangle' -$ induced spectral shift), the $\langle J_r \rangle \frac{B_\theta}{c}$ force should usually exceed the parallel Reynolds force $-\partial_r \langle \tilde{v}_r \tilde{v}_\| \rangle$. This observation may have significant implications for modeling of intrinsic rotation. Moreover, the perpendicular momentum flux projection may offer certain desirable properties vis-à-vis of the $\rho_*$ scaling. It is far from clear, however, how to reconcile the unavoidable $B_\theta / B_T$ scaling of $\langle J_r \rangle B_\theta / c$ with the Rice

scaling of intrinsic rotation (i.e. $\Delta v \sim W / I_p$).

iii.) $\langle \delta E_r \delta E_{\|} \rangle$ stresses which arise from polarization charge effects working in concert with the parallel acceleration nonlinearity. This mechanism has the interesting property that it does not involve $\langle V_E \rangle'$ or intensity gradients, and only requires breaking of symmetry by outgoing wave propagation, to render $\langle k_r k_{\|} \rangle \neq 0$ . Thus, it is a universal, albeit modest, process which is operative in *all* plasma confinement regimes [20].

Regarding $\langle \delta E_r \delta E_{\|} \rangle$ stress, this effect originates from the parallel nonlinearity in gyrokinetics as a consequence of polarization drift-induced charge separation. It may be viewed a type of polarization stress, and is termed residual since it does not depend on either flow or flow shear. The effective force emerges as a divergence of stress $\sigma_{r\|}$ as a consequence of the fact that polarization charge $\rho_{pol} \cong \nabla^2 \phi$ , so $\sigma_{r\|} \approx \langle \delta E_r \delta E_{\|} \rangle$. Symmetry breaking in the form of outgoing wave boundary conditions is required to render $\sigma_{r\|} \neq 0$.

The residual stress mechanisms discussed here are summarized in Table I. The reader should note that the residual stress mechanisms encompass, but are by no means limited to the traditional example of $E \times B$ shear symmetry breaking. Thus, we see that residual stress -and thus intrinsic rotation- are generic and ubiquitous physical entities directly linked to plasma turbulence, energy transport and relaxation.

| Wave Stress Mechanisms | Spectral Moment | Symmetry Breaking |
|---|---|---|
| Parallel Reynolds<br>$\left\langle \tilde{V}_{rE}\tilde{V}_{\|} \right\rangle$ | $\left\langle k_\theta k_\| \left\| \phi_{\underline{k}} \right\|^2 \right\rangle$ | $k_\| \rightarrow \begin{cases} \langle V_E \rangle' \\ \partial \langle N \rangle / \partial r \neq 0 \\ \text{(intensity gradients)} \end{cases}$ |
| $\langle J_r \rangle B_\theta / B_T \rightarrow$<br>$\frac{B_\theta}{B_T}\left\langle \tilde{V}_{rE}\tilde{V}_{\theta E} \right\rangle$ | $\left\langle k_\theta k_r \left\| \phi_{\underline{k}} \right\|^2 \right\rangle$ | $r \rightarrow \partial \langle N \rangle / \partial r \neq 0$<br>(intensity gradient)<br>$k_r \rightarrow \partial \langle N \rangle / \partial k_r \neq 0$<br>(spectral slope) |
| Polarization +<br>Parallel acceleration | $\left\langle k_r k_\| \left\| \phi_{\underline{k}} \right\|^2 \right\rangle$ | outgoing wave propagation |

Table 1. **The different wave stress and symmetry breaking mechanisms.**

## 2. Theory of the Toroidal Velocity Pinch

While residual stress is required to drive intrinsic rotation, a momentum pinch will contribute to rotation profile formation and peaking. The turbulent angular momentum flux carried by ions resonant with toroidal ITG turbulence has been calculated via quasilinear theory using a lab frame, phase space conserving gyrokinetic equation. Results near ITG marginality indicate that the *inward* turbulent equipartition (TEP) momentum pinch emerges as *the* robust pinch process. Regarding thermoelectric effects, results for typical parameters characteristic of the near marginal regime indicate that the ion $\nabla T$ -driven momentum flux is usually inward, while the $\nabla n$ -driven momentum flux is usually outward. Thus, these two fluxes tend to negate each other, leaving the TEP pinch as the robust survivor. Note that since tokamak plasma dynamics is not Galilean invariant (i.e. pinches are curvature driven), the issue of Galilean invariance constraints on the momentum pinch is moot [21].

Proceeding in more detail, we can in general write the momentum pinch velocity $V$ as:

$$V = V_{TEP} + V_{Th} \quad \textbf{(8)}$$

The TEP (turbulence equipartition) part is a consequence of compressibility of the **E**x**B** velocity in toroidal geometry (i.e. $\nabla \cdot \vec{v}_E \neq 0$). As a consequence,

$$\left(\partial_t + v_E \cdot \nabla\right)\left(n \frac{v_{\|}}{B^2} R\right) \cong 0 \quad \textbf{(8a)}$$

just as for density, it has long been known that [22]

$$\left(\partial_t + v_E \cdot \nabla\right)\left(\frac{n}{B}\right) \cong 0 \quad \textbf{(8b)}$$

i.e. *magnetically weighted* angular momentum and density are both conservatively advected by the **E**x**B** fluctuations. As a consequence, the relevant fluxes are driven by gradients of the locally conserved quantities, so

$$\Gamma_{L\phi} = -D_T \nabla\left(n \frac{v_{\|}}{B^2} R\right) \cong -D_T \nabla\left(\frac{L_\phi}{B^2}\right) \quad \textbf{(9a)}$$

and

$$\Gamma_n = -D_T \nabla\left(\frac{n}{B}\right) \quad \textbf{(9b)}$$

Here, $D_T$ is a generic turbulent diffusivity. Consequently:

$$\Gamma_{L\phi} = -D_T \left[\frac{1}{B^2} \nabla L_\phi - \frac{2}{B^3} L_\phi \nabla B\right] \quad \textbf{(10a)}$$

and

$$\Gamma_n = -D_T \left[\frac{1}{B} \nabla n - \frac{1}{B^2} n \nabla B\right] \quad \textbf{(10b)}$$

and we see the straightworward emergence of inward angular momentum and density pinches. Note that $\nabla B / B$ drives both inward fluxes. Lengthy analysis based on *rigorous* gyrokinetics supports the basic calculations of this simple conclusion, the main difference

being the numerical factor in front of the $\nabla B$ contribution. The TEP momentum pinch can also be obtained by considerations of homogeneization or mixing of toroidal angular momentum. Note that the physics of the TEP density and momentum pinch are *basically identical.* These two represent the irreducible minimum of turbulent inward pinches. Note, however, that the TEP momentum pinch is rather modest in that:

$$R\,V_{TEP}/\chi_{\phi} = -\alpha \qquad \textbf{(11)}$$

where $\alpha \cong 3$.

In addition to the basic and unavoidable TEP pinch, the momentum convection velocity also contains thermoelectric contributions, driven by $\nabla T_i$ and $\nabla n$ (nb: here we discuss ITG only). Thus,

$$V_{Thermoelec.} = \sum_{\|} \left|\tilde{V}_{r,\mathrm{k}}\right|^2 \tau_{c,\mathrm{k}} \left\{ g_1(\mathrm{k},\omega_{\|}) \frac{\nabla T_i}{T_i} + g_2(\mathrm{k},\omega_{\|}) \frac{\nabla n}{n} \right\} \qquad \textbf{(12)}$$

Here, $g_1(\mathrm{k})$ and $g_2(\mathrm{k})$ can each be positive or negative and reflect complex parameter dependencies. Note that superficially, $R\,V_{Th}/\chi_{\phi} \sim 0 \;\; (1/\varepsilon)$ so the thermoelectric pinch may *appear* more robust than the TEP pinch. However, reality is not so simple. Detailed gyrokinetic analysis reveals that close to ITG threshold (i.e. the relevant regime for stiff profiles), the $\nabla T$ -driven thermoelectric flow is *inward* (i.e. a pinch) but the $\nabla n$ -driven thermoelectric flux is *outward*. Thus, the two tend to compete with one another and cancel, *so the TEP pinch is, in fact, the most robust momentum pinch process.* The complex interplay and dependencies are summarized in Table.2 [23].

| For ITG : $V_{\text{pinch}}/\chi_\phi$ | $\nabla n$ driven | $\nabla T_{\text{i}}$ driven | $\nabla B$ driven |
|---|---|---|---|
| Fluid regime in torus | $-1/L_n$ Inward | 0 | $-4/R$ , for $\tau = 1$ Inward |
| Kinetic regime near marginality in slab | $1/L_n$ Outward | $-\left(\frac{1}{\eta_{\text{i}}^{\text{crit}}} + \Omega^2\right)/L_{T\text{i}}$ Inward | Ignored |
| Kinetic regime near marginality in torus (This work) | $1/L_n$ Outward | $-\left(\frac{5}{2} - \alpha_c(\omega_k)\right)/L_{T\text{i}}$ Inward | $-\frac{8}{5}\alpha_c(\omega_k)/R$ Inward |

Table 2. **Analytic predictions on momentum pinch. Note that the $\nabla T_i$ –driven momentum pinch is similar to the $\nabla T_i$ –driven particle pinch.**

## III. Summary of Computational results

This section presents the relevant computational results.

### i.Basic issues and approaches

All keepers of the codes were asked to:

a. Perform a Reynolds stress inventory, i.e. if $\left\langle \tilde{v}_r \tilde{v}_{\parallel} \right\rangle = -\chi_\phi \frac{\partial \left\langle v_\phi \right\rangle}{\partial r} + \Pi_{OD}$ , where $\Pi_{OD} = V\left\langle v_\phi \right\rangle + \Pi_{r,\phi}^{resid}$ then they should decompose the off-diagonal flux $\Pi_{OD}$ into pinch $V$ and residual stress $\Pi_{r,\phi}^{resid}$ pieces.

b. Explore the dependencies of the dimensionless quantities $R\,V/\chi_\phi$ and $R\,\Pi^{resid}/v_{Ti}\chi_\phi$, which are convenient dimensionless figures of merit of the strength of the various contributions.

Note that both figures of merit are independent of the turbulence amplitude. Scans of

$R/L_T - R/L_{T,c}$, zonal flow damping and $\langle v_E \rangle'$ were suggested. The aims were to:

1.Inventory $\Pi_{OD}$

2.Tabulate $R\,V/\chi_\phi$ and $R\,\Pi^{resid}/v_{Ti}\chi_\phi$ vs $R/L_T - R/L_{T,c}$

3.Use a scan of zonal flow damping to identify and elucidate mechanisms of $k_\parallel$ symmetry breaking *not* related to $\langle v_E \rangle'$, i.e. especially intensity gradients $\nabla_r I$

4.Scan $R/L_n$ for fixed $R/L_T$ to study $\nabla T_i$ vs $\nabla n$ competition in the pinch

**ii.gKPSP results**

Numerical studies have been performed using the global gyrokinetic code gKPSP to elucidate the role of $\langle V_E \rangle'$ on the generation of intrinsic rotation and the sensitivity of this mechanism to collisional damping. A set of simulations were performed by varying both $R/L_T - R/L_{Tc}$ and collisionality $\nu_*$. Concentric circular geometry was assumed for these simulations, together with the following parameters: $75 < a/\rho_i < 140$ , $R/L_n = 2.22$ , $3.14 < R/L_T - R/L_{Tc} \le 10$ , $0 \le \nu_* \le 0.085$ , $q = 1.4$ at $r = 0.5a$ . No slip boundary condition was imposed and the number of marker particles per Fourier mode kept was varied from 70 to 140. By assuming zero initial equilibrium flow, the stress component $\Pi_{r,\parallel}$ observed in the early stage of the simulations can be considered as the non-diffusive residual part i.e. $\Pi_{r,\parallel}^{resid}$ . Subsequently, a flow develops and then turbulent viscosity no

longer is negligible. Note that in gKPSP, the temperature gradient relaxes in the course of the simulation. Hence, the values of $R/L_T$ quoted must be regarded as only *initial*, and not average or typical values. Also, the diffusive contribution to the momentum flux was likely minimal due to $\nabla T$ relaxation.

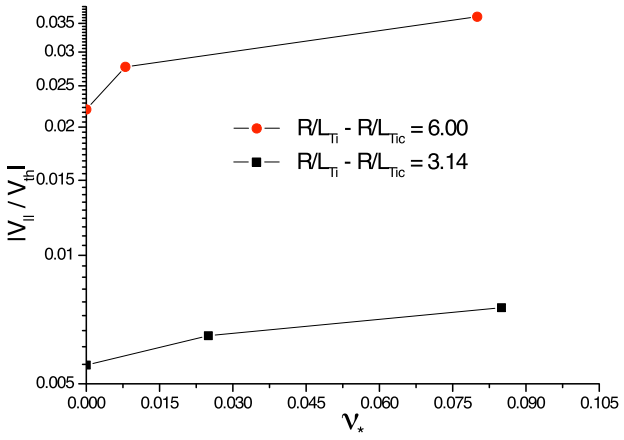


**Figure 2. Net (integrated) parallel flow level for different $R/L_{Ti}$-$R/L_{Tic}$ and collisionality.**

Fig. 2 shows the net flow observed in simulations for various $R/L_T - R/L_{Tc}$ and $\nu_*$ values. The aim of the collisionality scan was to provide an independent knob on $\langle V_E \rangle'$, via zonal flow damping. Here, $R/L_{Tc} \approx 4$ represents the linear instability threshold for these Cyclone-like parameters. With the increase in both parameters, the net flow generated by the residual stress was found to increase. According to current theory, the residual stress is expected to be proportional to the product of $\langle V_E \rangle'$ and turbulence intensity. Since the increase of $R/L_T - R/L_{Tc}$ enhances turbulence drive, and zonal flow

damping is also expected to increase the turbulence intensity on account of the 'predator-prey' character of their coupled evolution, the resulting increase of the net flow with $R/L_T$ is no surprise. Thus, to isolate the impact of zonal flow damping on intrinsic

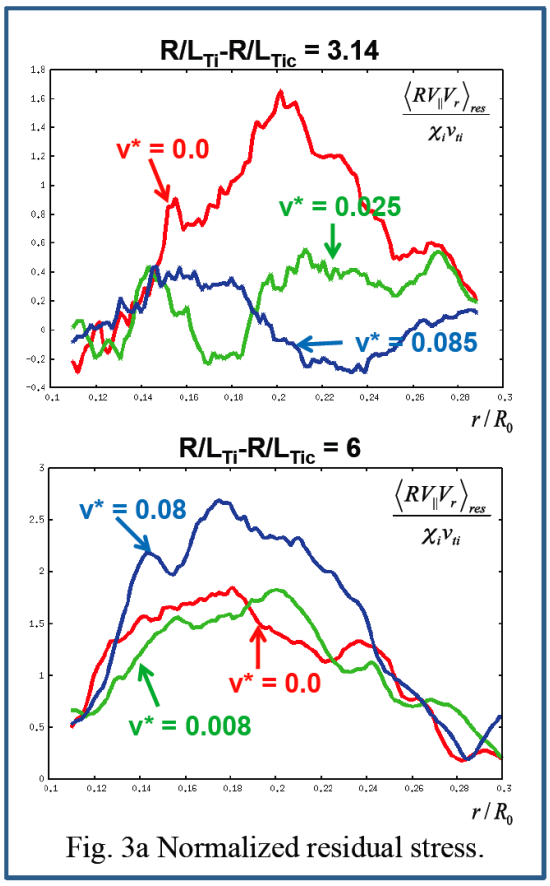


Fig. 3a Normalized residual stress.

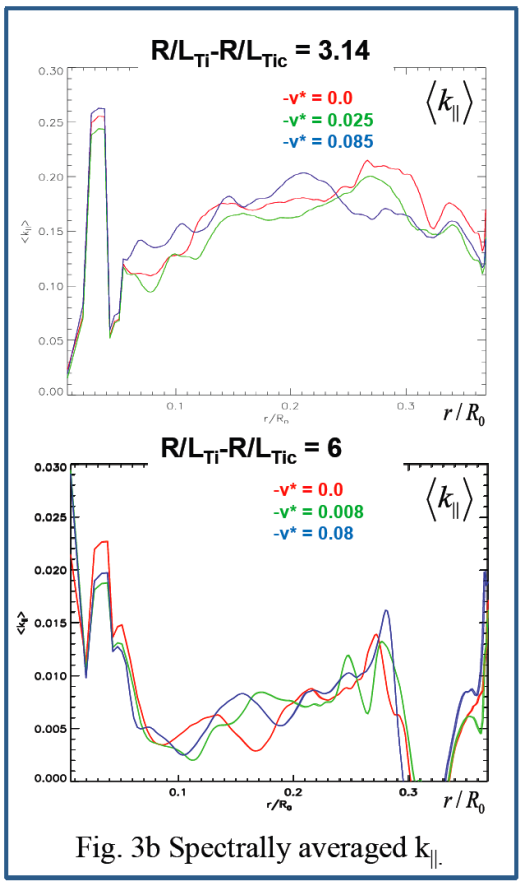


Fig. 3b Spectrally averaged $k_{||}$.

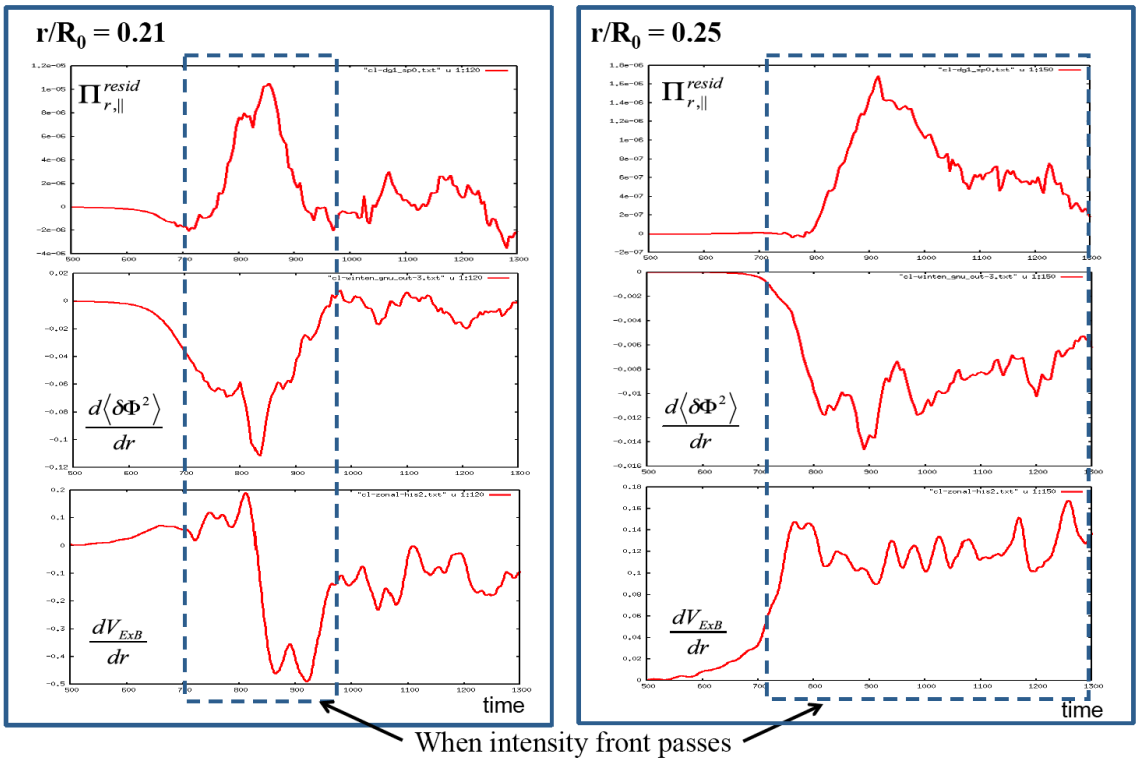


Fig. 4 Time history of residual stress, turbulence intensity gradient,
and zonal flow shear for propagating intensity in collisional environment.

rotation, we compensate for the direct proportionality of the residual stress to intensity by normalizing the stress by the thermal diffusivity $\chi_i$. Hence, we have examined the intensity-independent dimensionless ratio $R\Pi_{r,\|}^{resid} / V_{Ti}\chi_i$, the so called normalized residual stress. During the quasilinear phase of the evolution, fluctuation intensity profiles are similar for the values of zonal flow damping scanned. As a consequence, the normalized residual stress and mean parallel flow profile show similar behaviors for the scanned parameters. In the nonlinear phase of evolution, the collisionless case exhibits the largest $\langle V_E \rangle'$ and the smallest intensity level and the most collisional case exhibits the

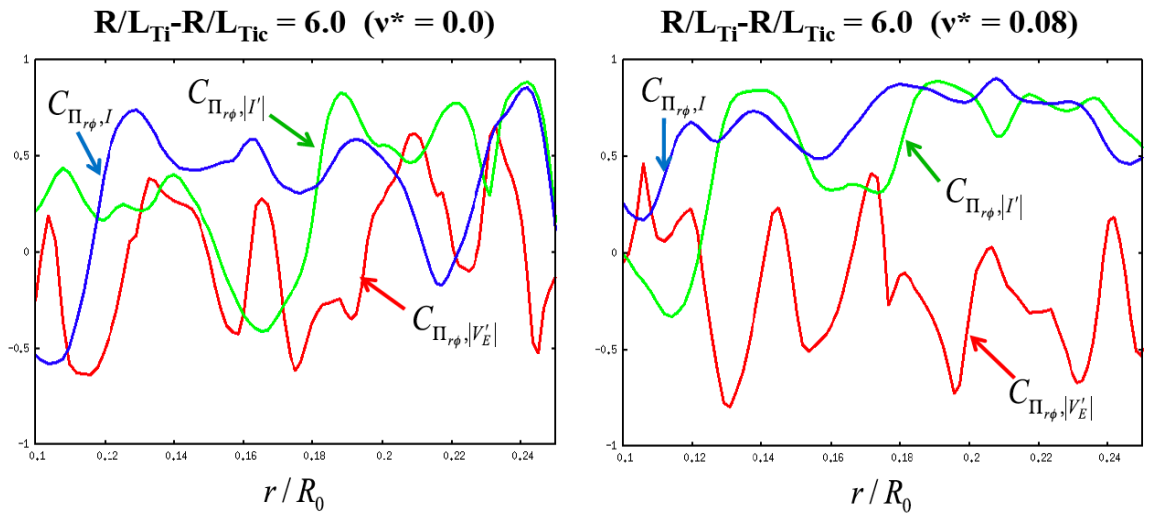


Fig. 5 Correlations between residual stress, turbulence intensity gradient, and zonal flow shear for collisionless and the most collisional case.

complementary extreme i.e. the smallest $\langle V_E \rangle'$ and the largest intensity level. *In Fig.3a, it is notable that appreciable normalized residual stress persists for all the cases, which means significant* $k_{\|}$ *symmetry breaking is still present when zonal flow damping is largest*, an inference confirmed by direct measurement of the spectrally averaged $k_{\|}$ (see Fig. 3b). The case with largest zonal flow damping supports a strong fluctuation intensity gradient, associated with an observed outward-propagating intensity front in the nonlinear phase. This front is probably due to profile relaxation and broadening. The normalized residual stress exhibits a correlation with the fluctuation intensity gradient, and tends to track the space-time evolution of the intensity (see Fig. 4).

For a more detailed study of the origin of symmetry breaking, we have examined the following correlation parameter between various physical quantities:

$$C_{X,Y}(r)=\frac{N\sum_{t=1}^{N}X(r,t)Y(r,t)-\left(\sum_{t=1}^{N}X(r,t)\right)\left(\sum_{t=1}^{N}Y(r,t)\right)}{\sqrt{N\left(\sum_{t=1}^{N}X^{2}(r,t)\right)-\left(\sum_{t=1}^{N}X(r,t)\right)^{2}}\times\sqrt{N\left(\sum_{t=1}^{N}Y^{2}(r,t)\right)-\left(\sum_{t=1}^{N}Y(r,t)\right)^{2}}} \quad \textbf{(13)}$$

Here $X(r,t)$ and $Y(r,t)$ denote the time history of physical quantity $X$ and $Y$, respectively, at discrete time points $t=1,2...,N$. $C_{X,Y}(r)$ gives the correlation information of two physical quantities over the discrete time duration $t=1\sim N$. Noting that strong positive correlation is implied by $C_{X,Y}(r)\sim 1$ and strong negative correlation by $C_{X,Y}(r)\sim -1$, we can see the difference of the origin of the symmetry breaking in Fig. 5. In this figure, the correlations between $\Pi_{r,\|}^{resid}$, $\left|V_E'\right|$, $I$, and $\left|I'\right|$ in nonlinear phase are compared for the cases with $R/L_T-R/L_{Tc}=6$. In the collisionless case, both $C_{\Pi_{r,\|}^{resid},|V_E'|}$ and $C_{\Pi_{r,\|}^{resid},|I'|}$ change their sign for different locations in minor radius, *implying a mixed or dual role of* $\left|V_E'\right|$ *and* $I'$ *in rotation generation!* However, the most collisional case shows a different qualitative tendency. $\Pi_{r,\|}^{resid}$ and $\left|I'\right|$ shows strong positive correlation over wide range of minor radius implying the *leading* role of $\left|I'\right|$ in rotation generation. The complementary negative correlation between $\Pi_{r,\|}^{resid}$ and $\left|V_E'\right|$ can be understood as the decrease of $\left|I'\right|$ by $\left|V_E'\right|$, which again implies a leading role for intensity gradients $\left|I'\right|$ in rotation generation.

Ongoing work for the next quarter includes the extended correlation analysis of various physical quantities to elucidate their role and dynamics in the intrinsic rotation generation. The analysis will be performed covering a wider range of parameter space. The verification of the present simulation results using enhanced computing resources is also planned.

**iii.GTS results**

Global gyrokinetic simulations using the GTS code have identified an important nonlinear flow generation process due to the residual stress produced by electrostatic turbulence of ion temperature gradient (ITG) modes and trapped electron modes (TEM) (Wang et al., to be submitted [24]). The residual stress is shown to drive intrinsic rotation as a type of wave-driven flow phenomenon which operates via wave-particle momentum exchange (Diamond et al, 2009[25]). Nonlinear residual stress generation by both the fluctuation intensity and the intensity gradient in the presence of broken $k_{\|}$ symmetry has been observed. Symmetry breaking in the parallel wave number spectrum induced by turbulence self-generated low frequency zonal flow shear has been identified to be a key, universal mechanism for driving residual stress (Wang et al, 2009). Simulations, particularly with kinetic electron physics included, also indicate the existence of other mechanisms beyond **E**x**B** shear for $k_{\|}$ symmetry breaking (Wang et al, 2009[26]).

**a. Nonlinear residual stress generation in ITG turbulence and impact of non-adiabatic electrons**

The physics picture of nonlinear residual stress generation is illustrated in Fig.6 which is

from a simulation of ITG turbulence in the marginal regime with adiabatic electrons. Typically, in ITG turbulence with adiabatic electrons, the nonlinearly generated residual stress is shown to drive a significant inward flux of toroidal momentum (upper-left panel), particularly in the post-saturation phase which is after the nonlinear saturation of

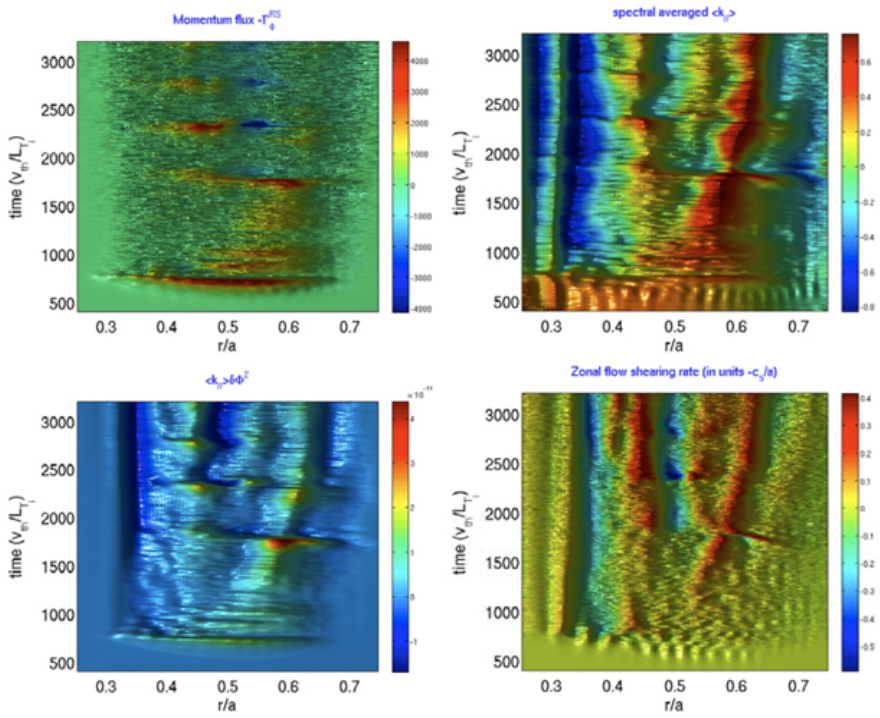


FIG.6 : Spatio-temporal evolution of radial flux of toroidal momentum (upper-left), $\langle k_{\|} \rangle \sum \delta\Phi_{mn}^2$ (lower-left), spectrum-averaged $\langle k_{\|} \rangle$ (upper-right) and zonal flow shearing rate (lower-right) from ITG simulation with adiabatic electrons. The major parameters used are: $R_0/L_{T_i} = 5.3$, $R_0/L_{T_e} = 1.6$ and $R_0/L_n = 1.0$.

the ITG instability, but before a long term steady state. Close spatio-temporal correlations among the momentum flux $\Gamma_\phi$ , $\sum k_{\|} \delta\phi_{mn}^2$ , which is a quantity resembling the residual stress expression, the spectrum averaged parallel wavenumber $\langle k_{\|} \rangle$ and the zonal flow shearing rate $\omega_E^{ZF}$ , as illustrated in Fig.6, clearly demonstrate that the residual stress is

nonlinearly driven by the fluctuation intensity acting with the zonal flow shear which induces symmetry breaking in the $k_{\parallel}$ spectrum. Since zonal flows are self-generated in most turbulence regimes, this process may represent a universal, nonlinear mechanism for residual stress generation. In particular, this is expected to play an important role in flow generation in core turbulence apart from internal transport barriers, i.e. in L-mode

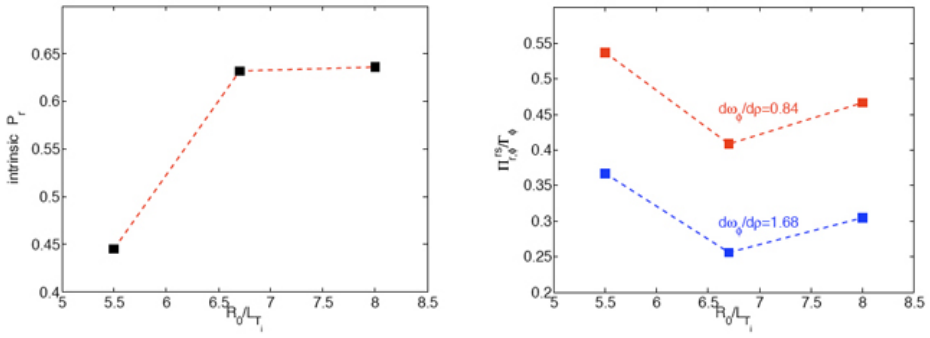


FIG. 7: Intrinsic Prandtl number versus $R_0/L_{Ti}$ (left) and the ratio of residual stress over total momentum flux versus rotation gradient and $R_0/L_{Ti}$ (right).

plasmas where the **E**x**B** shear of the equilibrium electric field is not dominant.

The characteristic dependence of non-diffusive momentum transport has been studied over a wide range of experimentally relevant parameters for the purpose of developing a predictive capability for plasma rotation in ITER. For typical tokamak parameters, the nonlinearly generated residual stress is shown to contribute up to more than 50% of the total momentum flux produced by ITG turbulence. The portion of the residual stress increases with the decrease of the rotation gradient (left panel of Fig.7). This is readily understandable because the residual stress, unlike the diffusive component, is independent of rotation gradient. The intrinsic Prandtl number, i.e., the ratio between momentum and ion heat diffusivity, is shown to increase with the ion temperature

gradient, specifically ranging from $P_r \sim 0.4-0.7$ for $R_0/L_{Ti} \sim 5.5-8.5$ (right panel of Fig.7). This result appears in general agreement with a recent theoretical prediction of $P_r \sim 0.2-0.5$ in stiff profile regimes. More importantly, the ``intrinsic" torque associated with residual stress is shown to increase close to linearly with the plasma

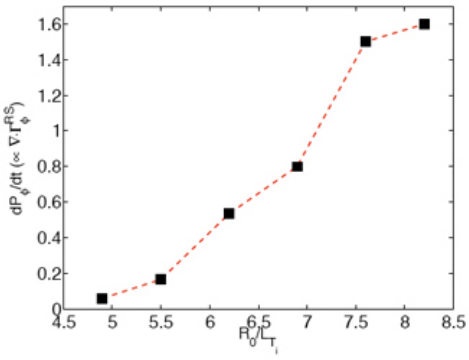


FIG.8 : Total intrinsic torque (spatially averaged) versus ion temperature gradient $R_0/L_{T_i}$.

pressure gradient, as is seen in Fig.8 from ITG simulations. The dominant underlying physics governing this scaling is that both the residual stress and the zonal flow shear increase with the turbulence intensity which, in turn, is increased with the strength of the ITG drive $R_0/L_{Ti}$. This result is consistent with experimental trends observed in various devices (Rice et al., 2009[27], Ida et al., 2009[28]), including C-MOD where the central flow velocity scales linearly with the edge pressure gradient.

The impact of kinetic electrons on the nonlinear residual stress generation has also been studied in ITG turbulence. The results of ITG turbulence with non-adiabatic electrons are presented in Fig.9 which uses exactly the same set of simulation parameters as in Fig.6. First, the weaker similarity of spatio-temporal structures between the directly

calculated momentum flux (residual stress, upper-left panel) and an estimate of $\sum k_{\|}\delta\phi_{mn}^2$ (lower-left) indicates that the latter, theoretically motivated residual stress does *not* fully account for the residual stress produced by the turbulence. Further, weaker

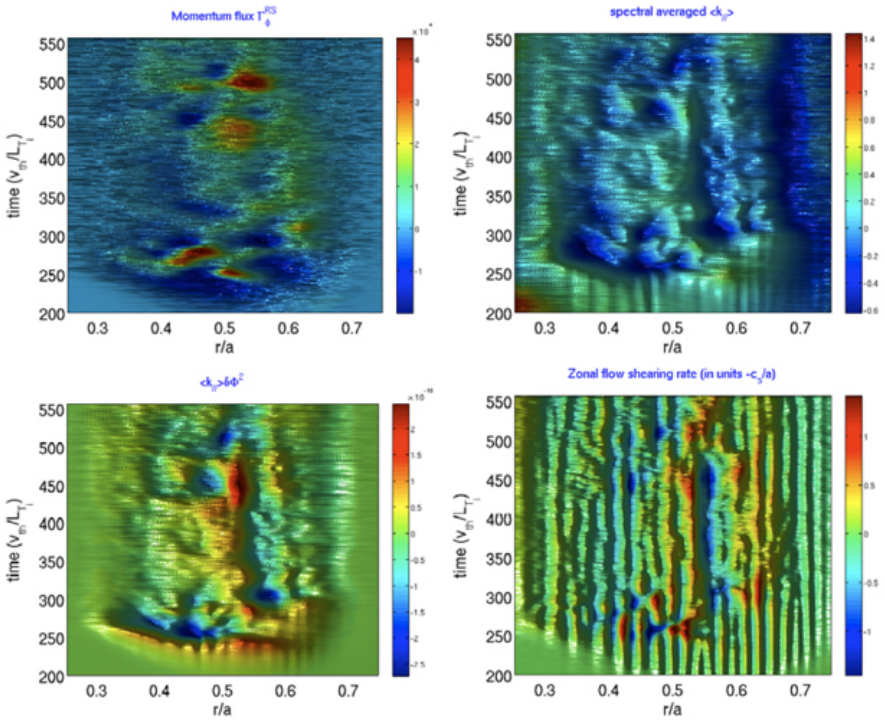


FIG. 9: Spatio-temporal evolution of radial flux of toroidal momentum (upper-left), $\langle k_{\|}\rangle \sum \delta\Phi_{mn}^2$ (lower-left), spectrum-averaged $\langle k_{\|}\rangle$ (upper-right) and zonal flow shearing rate (lower-right) from ITG simulation with nonadiabatic electrons.

correlation in spatio-temporal structures between $\langle k_{\|}\rangle$ (upper-right) and $\omega_E^{ZF}$ (lower-right) indicates that the zonal flow shear does not fully account for the origin of non-vanishing $\langle k_{\|}\rangle$. The non-adiabatic electrons are shown to introduce finer radial scales into the zonal flows. The corresponding **E**x**B** shear at small scales, however, appears too weak to have a visible impact on the $k_{\|}$ spectrum (upper-right and lower-right panels). The key points

made by these results clearly indicate: i) the likely existence of other possibilities, such as turbulence intensity gradient driven residual stress, and ii) the existence of other mechanisms beyond **E**x**B** shear for $k_{\|}$ symmetry breaking. For the latter, the possible mechanisms include the effects of magnetic shear, nonlinear mode

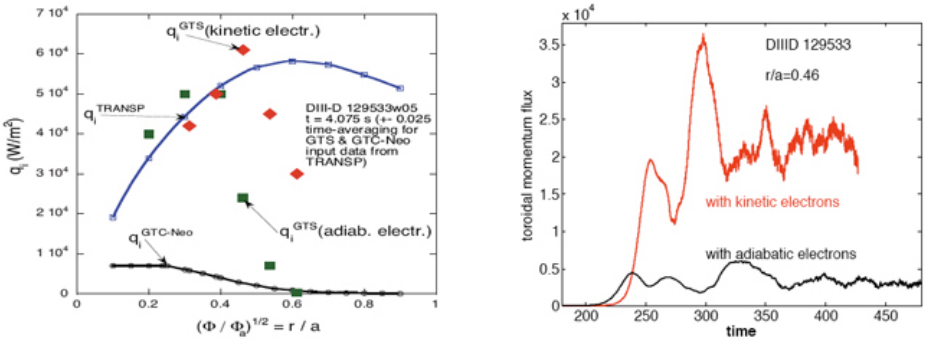


FIG.10: Ion heat fluxes vs $r/a$ from ITG simulations with adiabatic and non-adiabatic electrons and comparison with experimental results from TRANSP and neoclassical level from GTC-NEO (left); time history of ITG driven toroidal momentum fluxes, showing enhancement of residual stress due to trapped electrons (right).

couplings, and turbulent radial current, which will be investigated during the coming months.

On the other hand, in the ITG marginality regime, trapped electron physics is shown to play a critical role in determining plasma transport for the parameters of DIII-D plasmas, not only producing the proper ion heat flux in experiments but also substantially enhancing the residual stress generation (see Fig.10).

**b. Nonlinear residual stress generation in CTEM turbulence**

For typical plasma parameters of fusion experiments, collisionless TEM turbulence can be a major source to drive multiple-channel transport. The nonlinear residual stress generation by CTEM turbulence, for the first time, is clearly identified in global

simulations using typical parameters of DIII-D plasmas. This is elucidated in Fig.11 by close spatio-temporal correlations among the directly calculated $\Gamma_{\phi}^{RS}$ , $\sum k_{\|}\delta\phi_{mn}^{2}$ (a theoretically motivated quantity characterizing the turbulence intensity driven residual stress), $\langle k_{\|}\rangle$ , and $\omega_{E}^{ZF}$ .

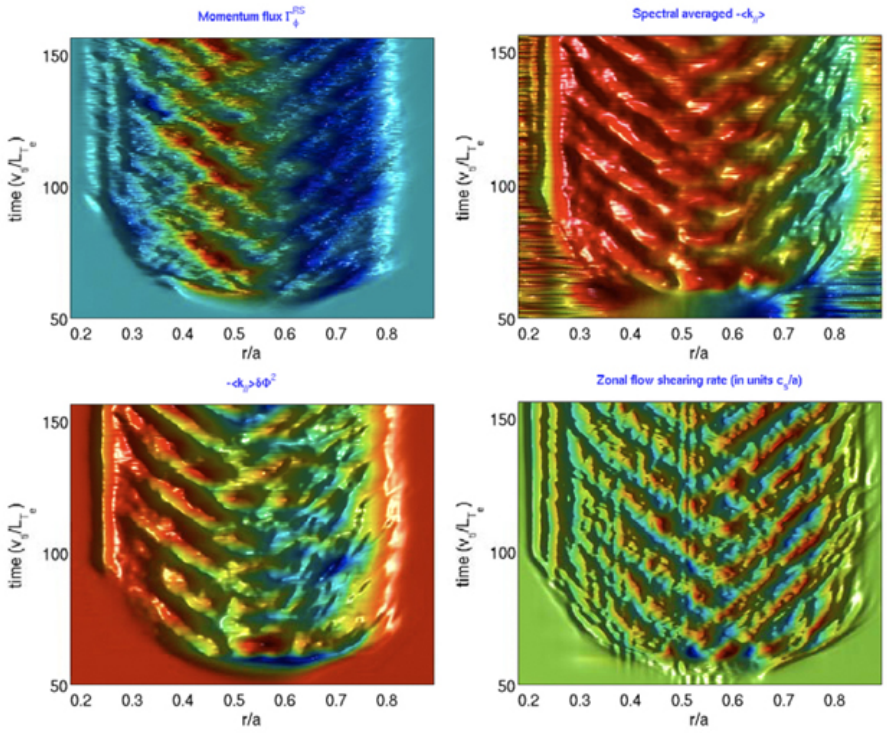


FIG.11: (Spatio-temporal evolution of radial flux of toroidal momentum (upper-left), $\langle k_{\|}\rangle \sum \delta\Phi_{mn}^{2}$ (lower-left), spectrum-averaged $\langle k_{\|}\rangle$ (upper-right) and zonal flow shearing rate (lower-right) from simulation of CTEM turbulence. The major parameters used are: $R_0/L_{T_e} = R_0/L_n = 6.0$, $R_0/L_{T_i} = 2.4$.

The residual stress at steady state changes direction from outward in the inner core region to inward in the outer core region. The turbulence intensity in the presence of non-vanishing $\langle k_{\|}\rangle$ is shown to play an important role in driving the residual stress, particularly in the inner core region ($r/a < 0.55$). In the outer core region ($r/a \geq 0.55$),

however, the turbulence intensity effect appears insufficient to well account for the residual stress generation.

The intensity gradients in both the radial direction and the wavenumber $k_r$ direction may act to drive a residual stress (Diamond et al., 2008[29]). Figure 12 shows the

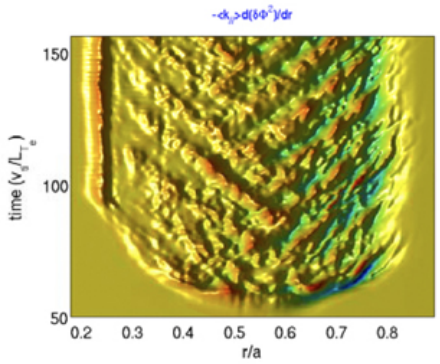


FIG.12: Spatio-temporal evolution of $\langle k_{\|} \rangle \sum \partial / \partial r (\delta \Phi^2)$ which represents a part of residual stress driven by turbulence intensity gradient.

spatio-temporal evolution of the quantity $-\langle k_{\|} \rangle \sum \partial / \partial r \left( \delta \phi^2 \right)$, which can be used to approximately represent the intensity gradient driven residual stress. Its apparent correlation with the directly calculated residual stress in Fig.11 is noted particularly in the outer core region where a significant effect of turbulence intensity is not observed. This simulation result is a clear identification of the turbulence intensity gradient driving residual stress in the presence of zonal flow shear induced symmetry breaking.

We also should point out that the meso-scale phenomena and their critical role in determining plasma transport and its radially nonlocal nature are highly pronounced in TEM turbulence. The CTEM turbulence and transport including the momentum flux are characterized by bursting events which emerge regularly in time and propagate radially

both inward and outward (see Fig.11). The bursting generation frequency and the radial propagation velocity are estimated to be $f_b \sim 0.1 c_s / a$ and $V_b \sim (5-10)\times 10^{-3} c_s$, respectively, where $c_s$ is the sound speed.

**iv. XGC results**

We now present simulation results from the full-f, flux-driven gyrokinetic code XGC1 (Ku et al., 2009[16]). We have especially focused our attention on the parallel velocity, on the total non-diffusive part of the parallel momentum (namely the sum of the residual stress $\Pi_{r,\|}^{resid}$ and the pinch $V\langle v_\| \rangle$) and tried to assess correlations between this non-diffusive residual and either (i) the **E**x**B** velocity shear $|V_E|'$, (ii) the turbulence intensity $I$, (iii) the turbulence intensity gradient $|I'|$, as well as (iv) the parallel velocity. No entirely unambiguous conclusions concerning the dependencies of the non-diffusive residual can be drawn from our data (see Fig.17). Essential differences with e.g. Fig.5 may reside in the fact that our system is (i) weakly turbulent, sitting at marginality ($R/L_T \sim 6$), thus displaying a low level of turbulence and a small intensity and intensity gradient. Also, (ii) while being driven by a heat flux, equilibration of the flows is a *long* process, which our simulation may not have yet accommodated, and during which corrugations, fluctuations, etc. of every profile are allowed. These effects likely contribute to the `unsettled'-like aspect of the results.

The temporal and radial traces of the parallel momentum flux are shown in Fig.13,

using Cyclone-like parameters comparable to those used by gKPSP, with a simulated $\rho_* \sim 1/184$. After an initial redistribution of parallel angular momentum that has seen transient inward and outward fluxes of this quantity, a quasi-stationary, slowly oscillating regime is reached, in which the momentum flux settles on averge, yet interestingly oscillates with time, quasi-periodically, *regularly redistributing parallel momentum both inwards and outwards*. The temporally averaged (during this quasi-periodic behavior) radial distribution of parallel momentum displays a smooth sine-like shape –close to zero on average throughout the whole box– as compared to the `choppy' initial radial profile which has developed and rearranges on a very short time scale. This behavior of the parallel momentum flux is to be compared to that of the parallel velocity, see Fig.14.

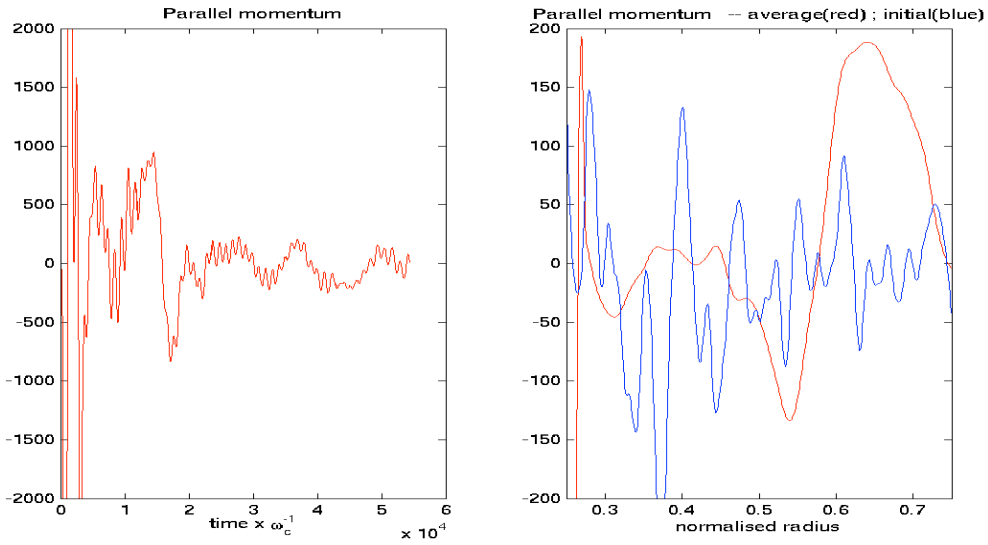


**Figure 13. Temporal (left) and radial (right) traces of the parallel momentum flux.**

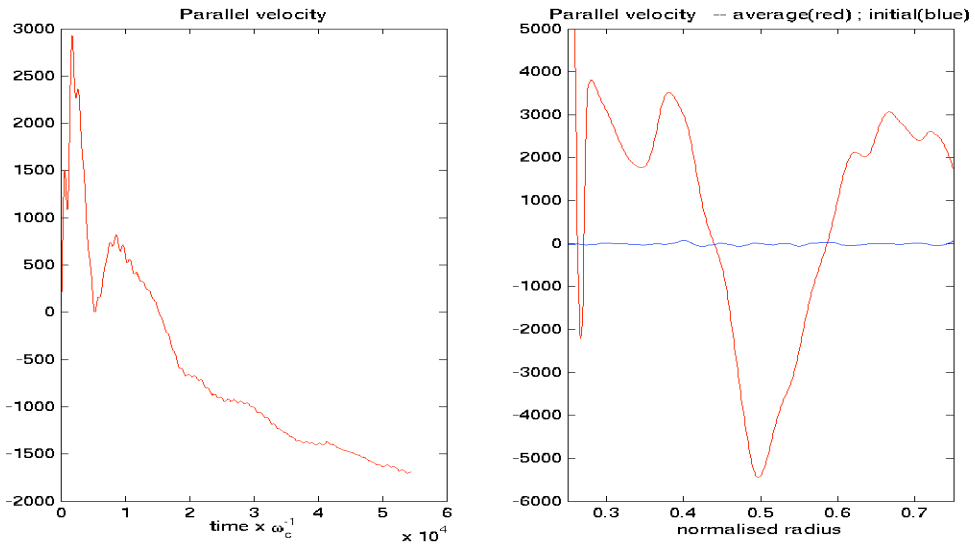


**Figure 14. Temporal (left) and radial (right) traces of the parallel velocity.**

One can immediately see that even though the transport of momentum in the parallel direction is in a quasi-stationary state and has occurred for a significant amount of time (several bounce periods), the temporal trace of the parallel velocity is still evolving and changing sign, suggesting that the velocity profile (which is not a conserved quantity) equilibrates on a time scale much longer than that of the momentum flux (a conserved quantity).

From the simulated electric potential, we then synthesize the turbulent radial velocity $\tilde{v}_r$ and compute the eddy correlation time $\tau_c$ (the autocorrelation time of quantity $\tilde{v}_{r,m>0}$, m being the poloidal mode number), following the procedure described in Yan et al., 2010. These quantities then allow us to synthesize the diffusive part of the momentum flux $\chi_{\parallel} = -\left\langle \tilde{v}_r^2 \right\rangle \tau_c \frac{\partial v_{\parallel}}{\partial r}$, *without supposing a Prandtl number* $\chi_{\parallel}/\chi_i \equiv \left\langle \tilde{v}_r^2 \right\rangle \tau_c / \chi_i$ *of order unity.*

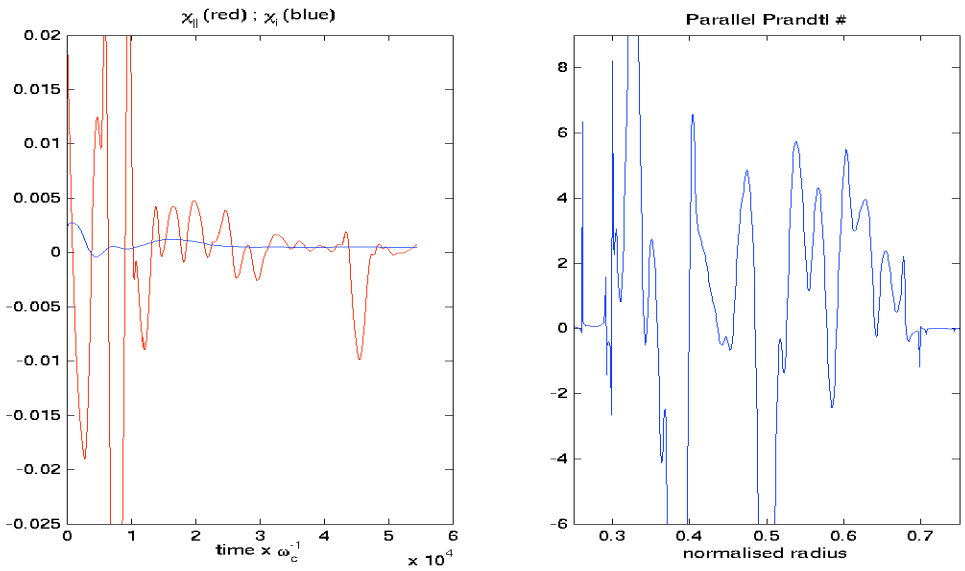


**Figure 15. Comparing the heat diffusivity and the diffusive part of the momentum flux.**

Figure 15 compares this diffusive parallel momentum flux to the heat diffusivity. After strong initial excursions, the radially averaged $\chi_{\parallel}$ settles close to $\chi_i$, meaning that in the momentum quasi-steady state the Prandtl number is of order unity, i.e. $\mathrm{Pr} \approx 1$. A more detailed analysis though shows strong transient departures from $\mathrm{Pr} \approx 1$, together with a structured radial profile of this Prandtl number, even in a quiescent phase like the one between $34{,}000 < t/\omega_c < 42{,}000$.

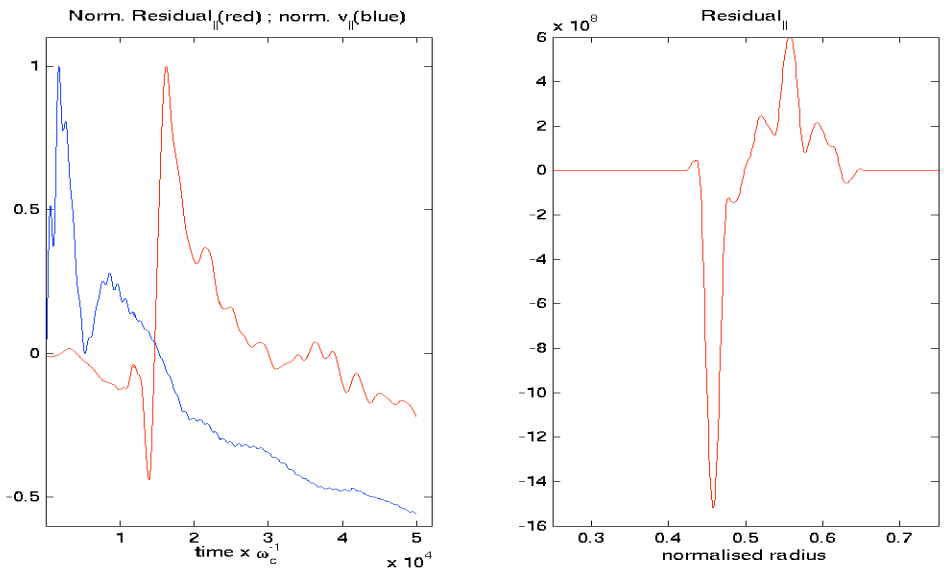


**Figure 16. Time trace of the non-diffusive parallel momentum flux and its radial structure.**

It is then straightforward to compute the non-diffusive part of the parallel momentum flux (hereafter referred to as the ``residual"): $\Re = \left\langle \tilde{v}_r^2 \right\rangle \tau_c \frac{\partial v_{||}}{\partial r} + \left\langle \tilde{v}_r \tilde{v}_{||} \right\rangle$, which contains both the pinch and the residual stress contributions: $\Re = V \left\langle v_{||} \right\rangle + \Pi_{||}^{resid}$. This quantity is plotted in Fig.16. Interestingly, it seems to track (with a delay) the temporal –and to some extent the radial structure also– of the parallel velocity. This fact suggests a non vanishing contribution of the pinch part to the non-diffusive parallel momentum flux. With the caveat –which we cannot develop further with the present data– regarding this non-diffusive part, we are still likely not to have converged to an equilibrium state, meaning that some rearrangement of non-diffusive parallel momentum might still be occurring. The idea extract from Fig.17 is that $\Re = V \left\langle v_{||} \right\rangle + \Pi_{||}^{resid}$ has low correlation with (i) the **E**x**B** velocity shear $\left| V_E \right|'$, (ii) the turbulence intensity $I$, (iii) the turbulence intensity

gradient $\left|I'\right|$, or (iv) the parallel velocity $\left\langle v_{\parallel}\right\rangle$ might thus not be conclusive, and should be regarded as characteristic of a transient.

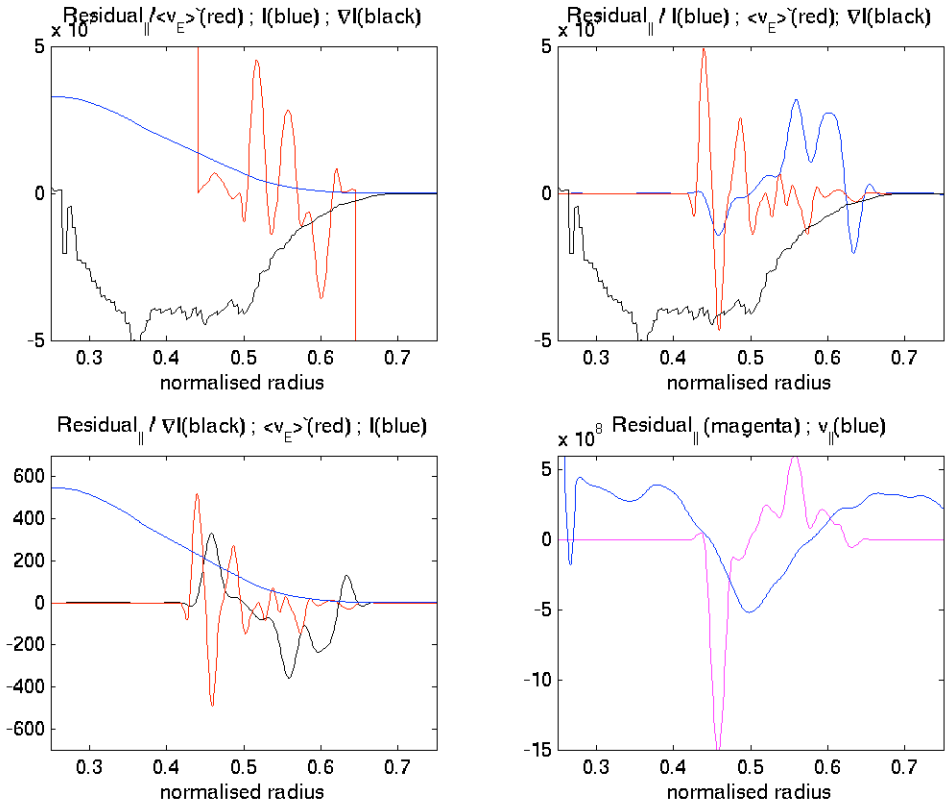


**Figure 17. Investigating the theory-predicted dependencies of the non-diffusive parallel momentum flux with velocity shear, turbulence intensity and parallel velocity.**

**v. Discussion of computational results**

Results from gKPSP, GTC and XGC were presented. All groups examined the residual stress $\Pi_{r,\parallel}^{resid}$ and the normalized residual stress $R\,\Pi_{r,\parallel}^{resid}/v_{Ti}\chi_{\phi}$. Specific findings include:

a. GTS ans gKPSP results showed the predicted clear correlation between residual stress, zonal electric field shear and intrinsic rotation. GTS results linked these to the effective mean $\langle k_{\parallel} \rangle$. These are all consistent with theoretical predictions

b. GTS results clearly showed that net intrinsic torque increases with $R/L_T - R/L_{T,crit}$, in qualitative agreement with the Rice scaling trend of $\Delta V \sim W/I_p$. We note, however, that current scaling was not examined.

c. gKPSP results demonstrate modest sensitivity of the intrinsic torque to ion collisionality, also in accord with experimental results. Furthermore, trade-offs in the residual stress between intensity and zonal shear were observed during a collisionality scan, consistent with the expected predator-prey interaction between zonal shear and intensity.

d. XGC results demonstrate an interesting disparity between the time scales for evolution of toroidal *momentum* and toroidal *rotation velocity*, in that the former approaches a stationary state much faster

than the latter does.

e. gKPSP results demonstrated the development of a correlation between the residual stress and the intensity gradient $\partial_r I$ as temperature gradient relaxation progressed and re-structured the profile. This is important as it establishes the viability of a second *universal* symmetry breaking mechanism.

f. GTS results confirm the theoretically predicted contribution of intensity gradient effects to residual stress in the presence of broken symmetry, i.e. $\Pi_{r,\parallel}^{resid} \sim \langle k_\parallel \rangle \partial_r I$.

g. XGC results suggest a flow or momentum pinch is at work, though further analysis is necessary.

h. GTS results demonstrated the persistence of an enhanced residual stress and intrinsic rotation in CTEM dominated regimes. This is important, as CTEM is expected to be active in ITER plasmas. This finding represents a challenge to theory.

i. Net turbulence-generated intrinsic rotation was observed in GTS, gKPSP and XGC studies, using no-slip boundary conditions. Volume-integrated angular momentum was shown to increase in all cases, though the magnitude of the increase varied.

j. Simulation studies, with the possible exception of XGC, did not suggest significant activity of a strong velocity pinch in the regimes studied. Future work should aim to elucidate and isolate this pinch physics by

study of cases with significant off-axis momentum input, resulting in large rotation velocities.

**IV. Conclusion**

All required performance targets for this quarter were met. In particular:

a. The physics of residual stress were elucidated. The electric field shear symmetry breaking mechanism was theoretically extended and elucidated, and confirmed by the detailed simulation studies. A new mechanism –namely symmetry breaking by intensity gradient– was proposed and identified in simulation results. A second residual novel residual stress mechanism, namely toroidal projection of the $\Pi_{r,\perp}$ stress was proposed.

b. Simulation results showed that intrinsic torque and residual stress both tended to increase with $R/L_T - R/L_{T,crit}$ and remain modestly sensitive to collisionality, in accord with experimental findings. Expected trade-offs between intensity and electric field shear, as predicted by predator-prey dynamics, is observed in the residual stress.

c. Intrinsic rotation development was confirmed in simulations. In particular, given a heat source, the net integrated momentum was observed to increase with time, for no-slip boundary conditions.

d. The existence of residual stress and intrinsic rotation was demonstrated for CTEM turbulence. The physics of the momentum pinch was elucidated theoretically. In particular, the decomposition of the pinch into TEP and thermoelectric was demonstrated, as was the fact that the TEP is the most

robust piece near threshold. Computationally, some evidence of a flow or momentum pinch at work is suggested, though further analysis is necessary.

e. The relation and close similarity between TEP momentum and density pinches was addressed and elucidated. The thermoelectric momentum pinch also resembles the corresponding density pinch.

This report contains several new results, which are:

i. The theoretical suggestion and computational demonstration of intensity gradients as a viable symmetry breaking mechanism, and the demonstration of the contribution of intensity gradients to residual stress.

ii. The computational demonstration that residual stress increases with $R/L_T - R/L_{T,crit}$ and is weakly dependent on collisionality.

iii. The computational demonstration of residual stress and intrinsic rotation for CTEM turbulence.

iv. The theoretical suggestion of toroidal projection of $\Pi_{r,\perp}$ as a residual stress mechanism.

v. The computational demonstration of the robustness of the residual stress to predator-prey type variations and trade-offs in fluctuation intensity and electric field shear.

vi. The theoretical demonstration that $\nabla T$ and $\nabla n$ -driven thermoelectric pinches will tend to cancel near marginality.

vii. The computational suggestion of an interesting disparity between the time

scales for evolution of toroidal *momentum* and toroidal *rotation velocity*, in that the former approaches a stationary state much faster than the latter does. These results track aspects of the predictions based on homogenization theory in ref. (6), though further analysis is necessary.

Areas where further work is needed include, but are not limited to:

a.) analysis of current scaling (via *q(r)* and other parameters) in $\chi_\phi$ , $V$ and $\Pi^{res}$. The aim is to uncover the fundamental physics behind Rice's current scaling.

b.) more thorough decomposition of $V$ from $\Pi^{res}$ in the off-diagonal flux. As noted above, studies with an external torque should be pursued to separate pinch from residual stress.

c.) efforts to improved understanding of the apparent enhancement of $\Pi^{res}$ in CTEM turbulence.

d.) more detailed quantitative comparisons and analysis of the various competing and related symmetry breaking mechanisms. Correlation analyses will be useful. In particular, the $\langle J_r \rangle$ driven mechanism merits deeper study.

e.) studies of $\Pi^{res}$ in reversed shear configurations.

References

[1] P.H. Diamond, et al, Nucl. Fusion 49, 045002 (2009)

[2] M. Yoshida, et al., P.P.C.F. 48, 1673 (2006)

[3] T. Tala, et al., IAEA FEC Proceedings (2008)

[4] A. Peeters, et al., Phys. Rev. Lett. 98, 265003 (2007)

[5] T.S. Hahm, et al., Phys. Plasmas 14, 042306 (2007)
T.S. Hahm, et al., Phys. Plasmas 15, 055902 (2008)

[6] O. Gurcan, et al., Phys. Rev. Lett. 100, 135001 (2008)

[7] E.S. Yoon, et al., Nucl. Fusion, In Press (2010)

[8] O.D. Gurcan, et al., Phys. Plasmas 14, 042306 (2007)

[9] R.R. Dominguez, et al., Phys. Fluids B5, 3876 (1993)
P.H. Diamond, et al., 15th IAEA FEC Proceedings, pp. IAEA-CN-60/D-2-II-6

[10] O.D. Gurcan, et al., In preparation (2010)

[11] C. Lee, et al., APS-DPP Conference, Atlanta (2009)

[12] Y. Camenen, et al., Phys. Rev. Lett. 125001 (2009)

[13] W. Solomon, et al., P.P.C.F. 49, B313 (2007)
W. Solomon, et al., submitted to Phys. Plasmas (2009)

[14] J.M. Kwon, et al., H-mode workshop proceedings, PPPL (2009)

[15] W. Wang, et al., Phys. Plasmas 13, 092505 (2006)

[16] S. Ku, et al., Nucl. Fusion 49, 115021 (2009)

[17] O.D. Gurcan, et al., Ref. 8

[18] P.H. Diamond, et al., Phys. Plasmas 15, 012303 (2008)

[19] P.H. Diamond and Y.B. Kim, Phys. Fluids B3, 1626 (1991)
P.H. Diamond, et al., PPCF, 50, 1 (2008)
C.J McDevitt, et al., submitted to Phys. Plasmas (2010)

[20] C.J. McDevitt, et al., Phys. Plasmas 16, 052302 (2009)

[21] I.H. Hutxhinson, arXiv:0904.4003 (2009)

[22] V. Naulin, et al., Phys. Rev. Lett. 81, 4148 (1998)

[23] E.S. Yoon, et al., see Ref. 7

[24] W. Wang, et al., in preparation (2010)

[25] P.H. Diamond, see Ref. 18

[26] W. Wang, et al., Phys. Rev. Lett. 102, 035005 (2009)
W. Wang, et al., APS-DPP Conference, Atlanta (2009)

[27] J. Rice, et al., APS-DPP Conference, Dallas (2008)

[28] K. Ida, et al., H-mode workshop proceedings, PPPL (2009)

[29] P.H. Diamond, see Ref. 18

[30] Z. Yan, et al., Phys. Rev. Lett. 104, 065002 (2010)